A Comparative Study of Yokeless and Segmented Armature versus Single Sided Axial Flux PM Machine Topologies for Electric Traction

Narges Taran, *Member, IEEE*, David Klink, *Student Member, IEEE*, Greg Heins, *Member, IEEE*, Vandana Rallabandi, *Senior Member, IEEE*, Dean Patterson, *Life Fellow, IEEE*, Dan M. Ionel, *Fellow, IEEE*

***Abstract*—This paper systematically compares two axial flux permanent magnet (AFPM) machines designed for a university student racing car application: a double–rotor single–stator yokeless and segmented armature (YASA) structure, and a single–stator single–rotor configuration. Both machines are optimized for minimum loss and active weight using 3D finite element analysis and the highest performing candidate designs are compared in more detail. The studies indicate that the benefits offered by the YASA configuration over the single–stator single–rotor machine are achieved only for specific designs that are heavier. For the design space with lower mass, albeit with increased losses, the Pareto front designs overlap. In this envelope, the YASA configuration demonstrates higher efficiencies at higher speeds, whilst the single-stator single-rotor is more efficient in high torque duty cycles. This shows the performance of the two machines is very similar and the choice is application specific. To validate the Finite Element Analysis (FEA) used in the optimization, a prototype was built and tested. Results showed good alignment between simulation and experimental data.**

***Index Terms*—Axial flux permanent magnet, yokeless and segmented armature, YASA, single sided, topology advantages, multi–objective optimization, 3D FEA.**

I. Introduction

The disc shape of axial flux permanent magnet (AFPM) machines have opened up many configuration possibilities including yokeless and segmented armature (YASA). A review of axial flux technologies, including the various topologies was performed by Capponi et al [1]. The YASA machine can be regarded as a next generation Torus type AFPM machine [2], [3] that combines winding arrangments of the NN and NS type Torus machines. The YASA structure has been proposed for traction application [4] and gained attention due to its high torque density and the segmented stator teeth structure that facilitates higher slot fill factor.

Previous studies have compared the performance of the YASA machine with other axial and radial flux machines [5]–[7], or compare different axial topologies utilising soft magnetic composite (SMC) cores [8]. However whilst there has been work on optimisation of individual designs [9], optimal designs have not been considered for comparison, which may make the outcomes of such comparisons debatable. Recent work on axial flux machine design has been predominantly focused on YASA style machines, considering multiple different areas including: soft magnetic materials such as SMC or Amorphous alloys [8]–[11], structural analysis [12]–[15], thermal management [11], [15]–[19], manufacturing challenges including eccentricity and alignment [10], [11], [20], [21], and multi-physics studies [10], [15]. Optimal machine design will vary based on the application. This study will focus on optimising for electromagnetic material mass and loss, which are the critical parameters for the chosen application. This study presents the conditions that define which topology will be superior.

In this regard, this paper extends previous work [22], presenting a systematic comparison for an example traction application of the two machine structures shown in Fig. 1. Optimization studies for both machines are performed to simultaneously achieve the objectives of minimum active material mass and minimum electromagnetic loss, including the stator core loss and the DC copper loss. Due to the 3D flux path of the AFPM machines, 3D finite element analysis (FEA) is required for accurate performance estimation. Therefore, a surrogate assisted optimization process is employed that is capable of utilizing 3D FEA models for design evaluation. A comparative study is conducted for the optimum designs located on the Pareto front.

The next section describes the optimization method employed in this paper. Section III illustrates the AFPM machine topologies and their specifications for the optimal design. Section IV compares the obtained Pareto fronts and selected representative designs. Section V focuses on experimental validation and analyses. The last section of the paper is devoted to concluding discussions.

II. Kriging Surrogate Model Assisted Optimization

Three-dimensional FEA models provide the basis for an accurate design evaluation methodology, particularly for a machine with 3D magnetic flux or leakage flux path. In order to utilize time consuming 3D FEA models in the optimization process, a surrogate assisted algorithm is utilized, such as the one proposed in [23]. This is a two-level surrogate-assisted algorithm taking advantage of differential evolution

N. Taran and V. Rallabandi were with the SPARK Laboratory Department of Electrical and Computer Engineering, University of Kentucky, Lexington, KY 40506 USA and they are now with BorgWarner Inc., Noblesville Technical Center, IN and with GE Research, Niskayuna, NY, respectively (e-mails: narges.taran@ieee.org and vandana.rallabandi@ieee.org). D. M. Ionel is with the SPARK Laboratory, Department of Electrical and Computer Engineering, University of Kentucky, Lexington, KY 40506 USA (email: dan.ionel@ieee.org). D. Klink is with the Monash University, Clayton, VIC, Australia (email: david.klink@monash.edu). G. Heins and D. Patterson are with the Regal Beloit Corporation, Australia, Rowville, VIC 3178, Australia (e-mails: greg.heins@regalbeloit.com; dean.patterson@regalbeloit.com).

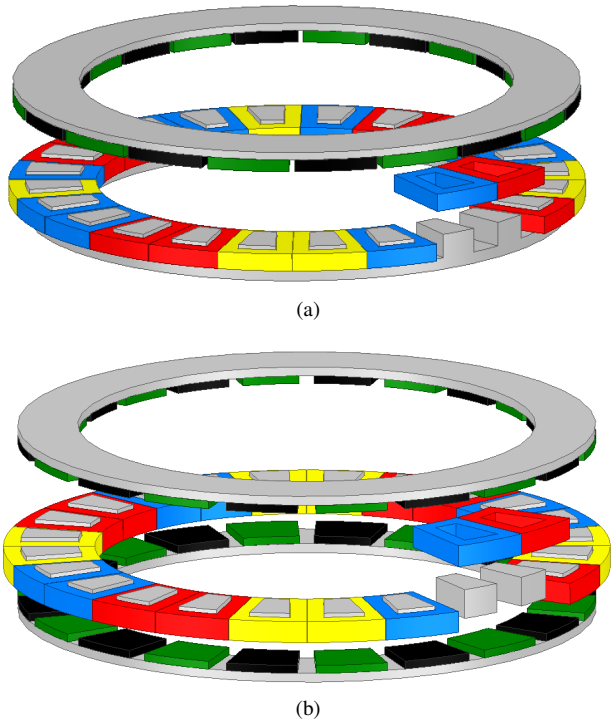

(a)

(b)

Fig. 1: The 3D parametric models of the two AFPM machines under study: (a) single–stator single–rotor, and (b) YASA with two rotors.

and kriging models. The kriging models can be defined as interpolations of sampled data points that are composed of two elements; trend and residual component. The trend component can be a polynomial regression model while the residual component reduces the estimation errors by increasing the weight of closer neighbor samples. This can be formulated as

$$\hat{Y} = \hat{X}\beta + r^T R^{-1}(Y - X\beta) \ , \tag{1}$$

where $\hat{X}$ is the design vector to be evaluated; $\hat{Y}$, response to be predicted based on the known sampled data points, i.e. X and Y. β is the matrix of regression coefficients that can be obtained using methods such as least squares. Kriging weights, r^T and R^{-1} are derived from the covariance function or semi-variogram and maximum likelihood estimation (MLE). The covariance function can be defined by various kernel functions, in this study Matern covariance function is employed [24].

This optimization flowchart, represented in Fig. 2, is based on a two level layout that provides an approach to evaluate only the most promising designs with computationally expensive 3D FEAs in the exterior loop, while the interior loop provides an approach for evaluating thousands of designs using inexpensive kriging surrogate interpolations. Considering that this approach drastically reduces the required number of FEA evaluations, it facilitates the application of 3D FEA. The algorithm is discussed in more detail in [23].

III. Design Topologies and Setup

The study reported here includes two AFPM machines, namely, a surface mounted (SPM) single sided 1–stator 1–rotor machine, shown in Fig. 1a, and a YASA machine

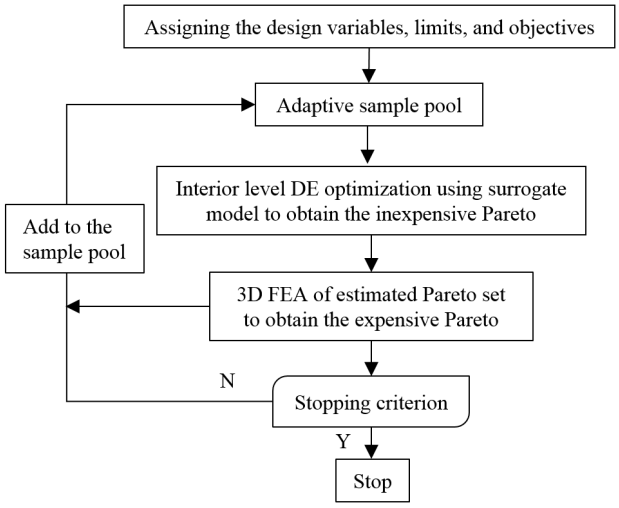

Fig. 2: The flowchart of the surrogate assisted optimization algorithm employing 3D FEA models.

TABLE I: Independent optimization variables and their corresponding limits.

Variable	Description	Min	Max
L_{ax}	Total axial length [mm]	25.0	40.0
k_{ry}	rotor yoke ratio = $\frac{L_{ry}}{L_{ax}}$	0.1	0.16
k_{sy}	stator yoke ratio = $\frac{L_{sy}}{L_{ax}}$	0.13	0.20
k_{pm}	magnet length ratio = $\frac{L_{pm}}{L_{ax}}$	0.18	0.24
k_{ds}	split ratio = $\frac{ID_s}{OD_s}$	0.58	0.86
k_{oh}	over hang ratio = $\frac{(OD_r - OD_s)}{(OD - OD_s)}$	-1.00	1.00
k_{sw}	slot width to slot pitch ratio = $\frac{w_s}{\tau_{s,id}}$	0.58	0.88
k_p	pole arc to pole pitch ratio = $\frac{\tau_{pa}}{\tau_{pp}}$	0.64	0.96

configuration, represented in Fig. 1b. The motors are optimally designed for an all-wheel-drive application in the Formula SAE (run by the Society of Automotive engineers) racing car design competition, also known as Formula Student in Europe. Both machines are rated to 70 Nm maximum torque and have a maximum speed of 6500 rpm.

In the optimization study, the current density is varied from design to design such that all produce the rated torque. Both machines incorporate 24 slots and 20 poles, concentrated winding and surface mounted magnets. The use of open slots and the application of bobbin wound coils result into the same high fill factor for the single sided machine as the YASA.

The motors are optimized employing accurate 3D FEA models for design evaluations. The objectives are to minimize active material mass and the electromagnetic loss, including the stator core loss and the DC copper loss. The winding and PM eddy current losses are estimated for the selected optimum designs.

The optimization process takes 8 variables for the single sided topology and 7 for the YASA, which features one less due to the absence of the stator yoke. The independent optimization variables are listed in Table I and shown in Figure 3.

The diameter being the most influential design variable, the optimization is conducted for two constraint diameters. The outer diameter is fixed at 200 mm and 300 mm for two

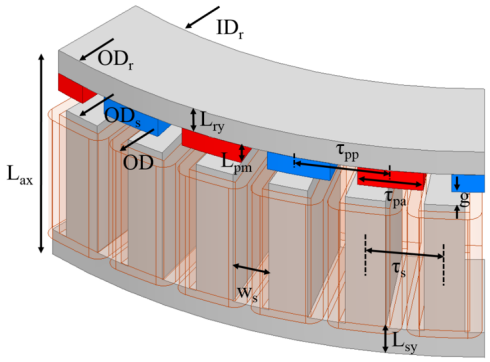

Fig. 3: The variables for the parametric model outlined in Table I.

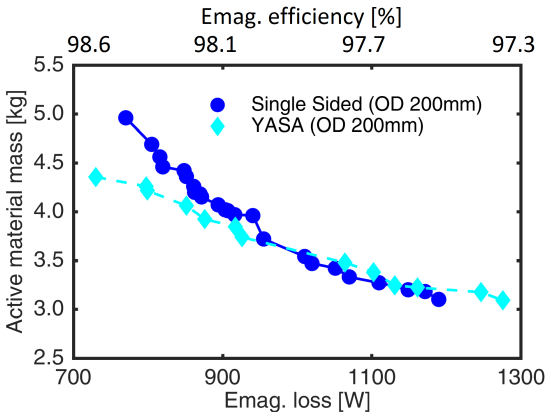

Fig. 4: The Pareto fronts for the topologies optimally designed for different envelopes: (a) outer diameter of 200 mm, (b) outer diameter of 300 mm.

sets of studies. This incorporates the effect of the motor's physical dimensions on the best choice. The non-dominated or Pareto front optimum designs are obtained and plotted (Fig. 4). Elaborated comparative discussions in the following sections are based on the optimal designs on the Pareto front.

IV. Comparative Study

A. Pareto front designs

The optimum designs from Fig. 4 produce the same rated torque, therefore a design with higher active material mass has lower specific torque (Nm/kg). It can be observed that for the designs with electromagnetic efficiency greater than about 98%, the YASA topology has a higher specific torque compared to the single sided one. On the other hand, this high efficiency zone of the design space includes heavier machines. In applications where the mass is a vital concern, the right side of the plots in Fig. 4 would be more of interest. In this case, the single sided machine has slightly higher specific torque. Based on these results, it may be noted that generally claiming higher specific torque for the YASA topology does not hold true, as it is the case only for very low loss designs.

For both the envelope dimensions studied, i.e. OD of 200 mm and 300 mm, the comparative performance represents a similar trend: for a mass sensitive application, the single sided topology may be at an advantage. In addition to the reduced mass, the single sided also has a higher capability to deal with the associated increased loss, as the stator is more accessible for cooling. On the other hand, if very efficient designs are of interest, higher specific torque can be gained by employing the YASA topology. The machines designed at a larger diameter constraint, can achieve even larger efficiency, albeit at the cost of increased mass.

The detailed distribution of optimization variables for the designs on the Pareto front is provided in Fig. 5. Some of the observations specific to this study are that the optimally designed YASA compared to single sided machines tend toward larger split ratios and slot widths. This may be explained by considering that the YASA topology has a lower stator core loss, due to the absence of the yoke, and hence higher flux density in the stator may be permissible, and thus, the machine can afford thinner teeth and therefore larger slot widths and split ratios. Additionally, the absence of the yoke may also contribute to this trend, allowing for higher tooth flux densities due to reduced slot leakage. It is expected that this trend would be amplified when utilising Grain Oriented Silicon Steel (GOSS) for the YASA machine. Torque ripple is not optimised in this study as it is usually relatively low for concentrated SPM machines, and the application (motorsport) is not sensitive to noise. The no load results have been included in table II. The YASA machine has slightly higher torque ripple, due to the high arc ratio.

In order to derive more general design guidelines and establish the limitations of the two topologies, the geometrical variables of the obtained Pareto designs are carefully investigated. For instance, the slot width and depth of the YASA machines were found to be larger than for the single sided ones, as shown in Fig. 6. A larger slot depth in the case of the single sided machine may not be beneficial as this also increases the leakage, more significantly than in the YASA machine. Considering the slope of the trend lines in Fig. 6, it can be inferred that lower loss and higher mass designs on the Pareto front generally have deeper slots and reduced slot width.

The performance of the evaluated designs in the optimization are later investigated in the three most frequent operating points. These points include the maximum condition (70 Nm and 6500 rpm) which the optimization was performed at, as well as 14 Nm and 35 Nm. Then each objective function for each design is calculated based on a weighted sum of that

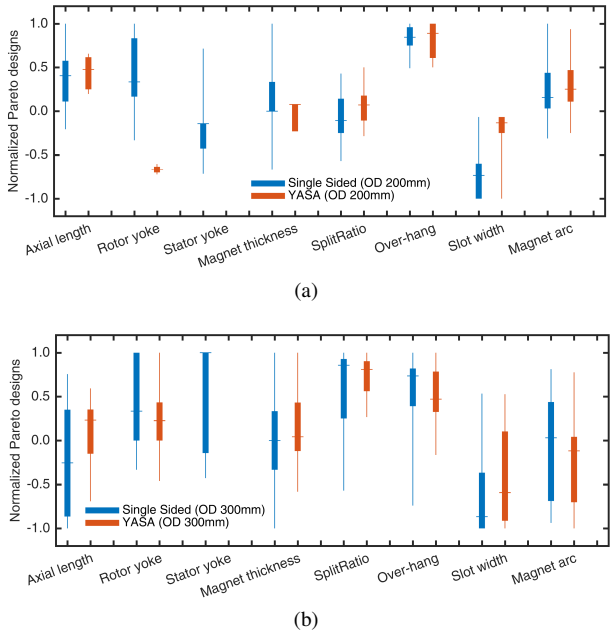

Fig. 5: The distribution of variables for optimum designs with total outer diameter of (a) 200 mm, (b) 300 mm.

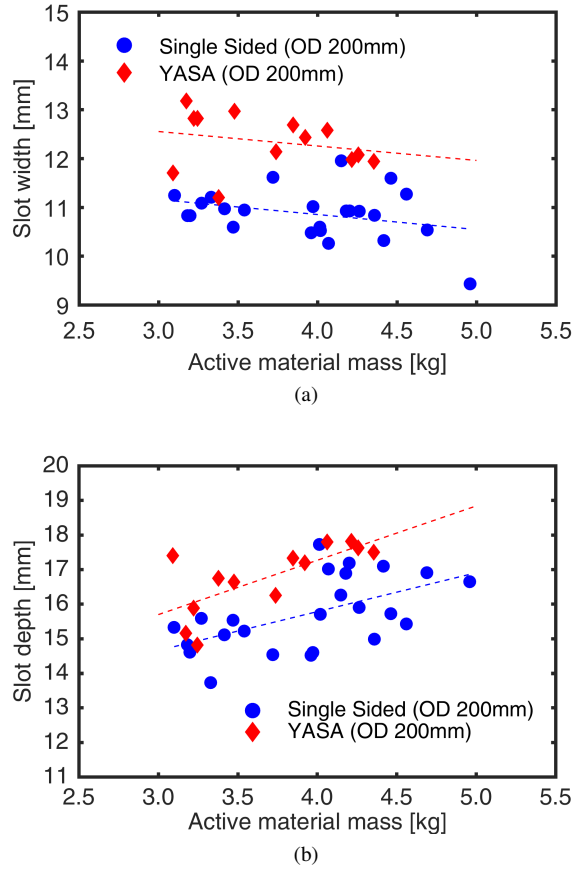

Fig. 6: The slot width and depth variation of Pareto front designs of (a) the single sided and (b) the YASA machine.

objective value in the three operating points. The weighting was assigned based on a duty cycle estimate. It was observed that the selected designs remain very close to the Pareto front.

B. Mass components breakdown

The breakdown of mass components for designs on the Pareto front is shown in Fig. 7. The copper mass required for optimum designs of the YASA machine is larger than for the single sided machine throughout the whole Pareto front. The magnet mass required for the optimum YASA design is also larger, except in designs with low total losses. It is interesting to note that the optimisation resulted in a very large arc ratio (0.93) for the YASA configuration, and a comparatively smaller arc ratio for the singled-sided (0.69). This can be attributed to the increased leakage that is present in the single-sided, due to its thicker magnets. The stator core mass of the YASA is smaller due to the elimination of the yoke, on the other hand it has higher rotor mass due to the two rotors.

Alongside the mass of the active electromagnetic material, there are differences due to ancillary components, however neither configuration is universally lighter. Whilst the single sided machine has added mass due to the aluminium backing required for mounting the stator, this is compensated by the additional rotor of the YASA machine, which also requires a similarly sized aluminium backing. The shafts of both the YASA and Single sided are required to take similar axial and torsional loads, and therefore are reasonably comparable in terms of mass. Assuming the YASA rotors are exposed, the housing and cooling mass of both will be relatively similar. The additional support structure required for the YASA due to the lack of a stator yoke will incur some additional mass, however the YASA configuration can afford slightly smaller bearings due to the lower axial loading, leading to a slightly lower mass which offsets this.

C. Loss components breakdown

The breakdown of loss components for designs on the Pareto front is presented in Fig. 8. It is observed that the copper loss is dominant in the case of both topologies with the ratings and envelope size under study. The copper loss of the optimally designed YASA machines is higher than that of the single sided ones, except for the very heavy and high efficiency designs. The stator core loss of the single sided topology is larger than the YASA for all the designs on the Pareto front, due to the added stator yoke loss. This discrepancy would grow further if utilising GOSS in the YASA configuration.

Two machines with similar mass and efficiency are selected in order to compare their key characteristics, including mass distribution, power factors, PM and winding eddy current losses, and their overall efficiency maps. The key parameters of both optimised designs can be seen in Table II. Eddy current losses are not considered in the optimization in order to accelerate the 3D design evaluation process. These losses are assessed for the two selected optimal designs as follows.

The topology under study employs sintered Neodymium magnets. Magnet eddy current loss calculation with 3D time-transient FEA for the selected optimally designed AFPM and YASA machines is shown in Fig. 9. Should only one magnet per pole be used in the rotor, the eddy-current losses would be extremely high at 1kW for the selected single sided topology and about twice that for the selected YASA topology. In

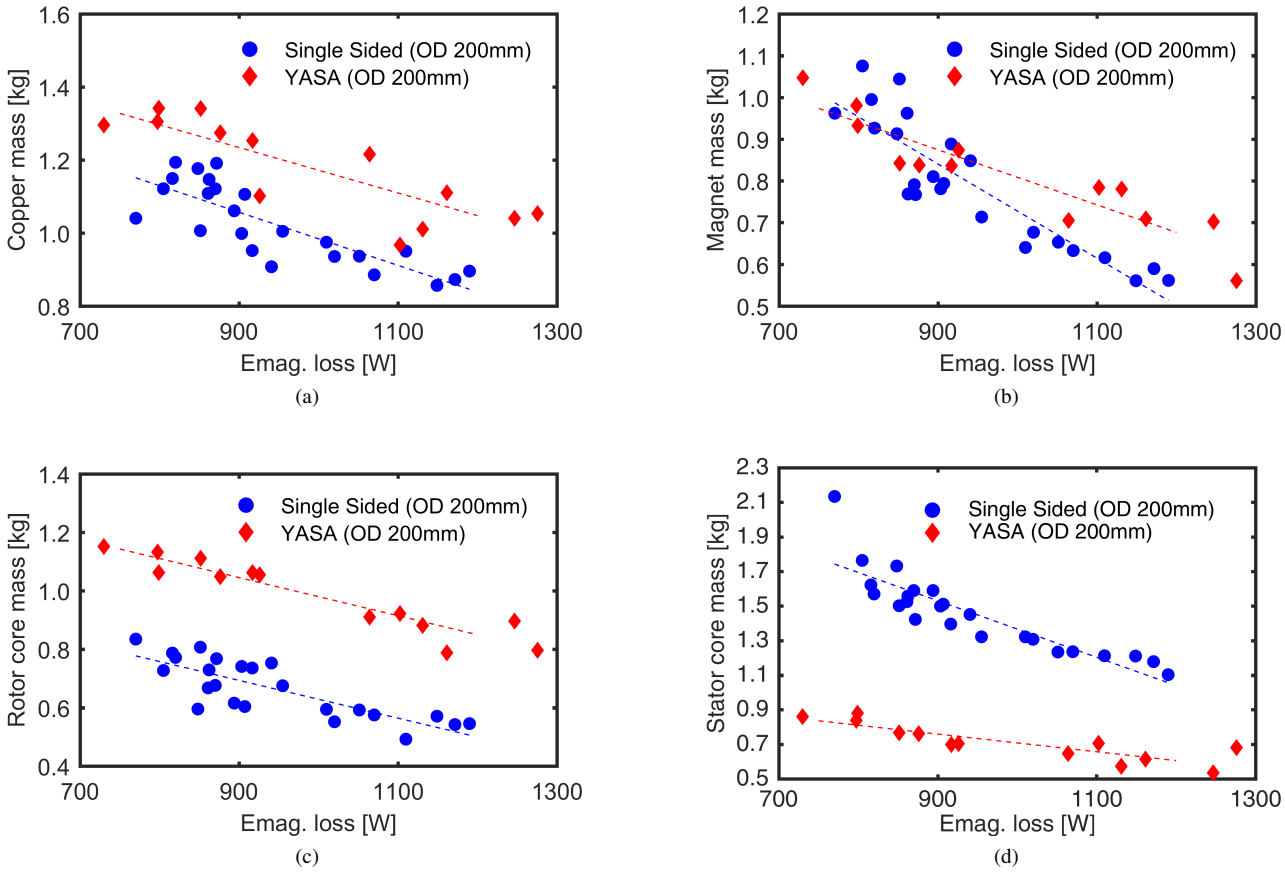

Fig. 7: The breakdown of mass components for the Pareto front designs of the topologies studied for an outer diameter of 200 mm. Similar trends were observed for the machines designed for the larger envelope with an outer diameter of 300mm.

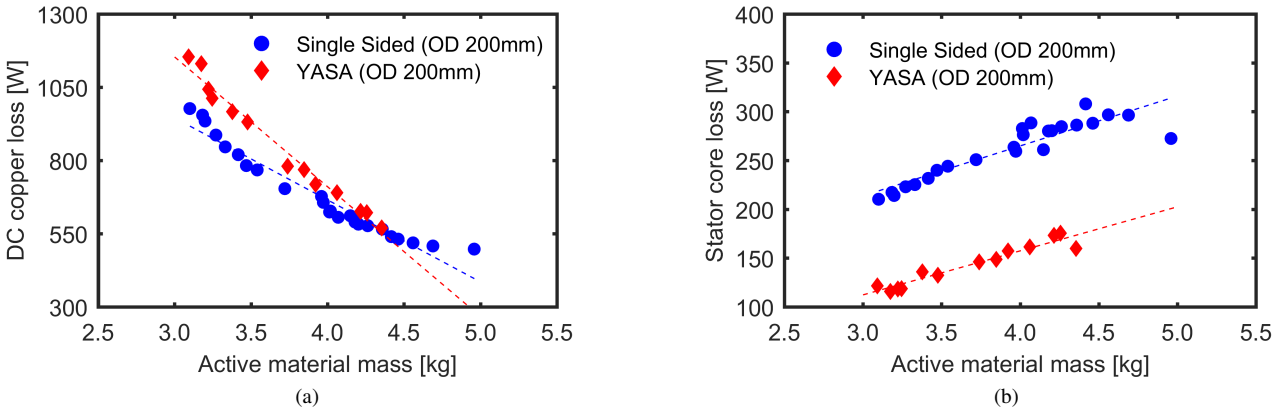

Fig. 8: The breakdown of loss components for Pareto front designs of the topologies studied for an outer diameter of 200 mm. Similar trends were observed for the machines designed for the larger envelope with an outer diameter of 300mm.

the practical design each pole is segmented in 10 magnet pieces, resulting in a drastic reduction of losses, rendering them negligible.

The reasons for larger PM loss for the YASA machine topology include: thinner magnets that reduce the permeance coefficient, and double the air gap magnet surface area which is exposed to the stator slotting and MMF harmonics. These show that for this design problem, magnet segmentation or other magnet loss reduction methods need to be taken into account, particularly for the YASA machine.

The winding eddy current losses for the two selected optimum designs at rated operating conditions are calculated in a 2D ANSYS Maxwell FEA model. The calculations are conducted for scenarios with different numbers of turns, all with AWG 12. The design is investigated with several winding arrangements, reducing the turn count by 3 in each iteration. The current density is readjusted for the rated torque. The FEA results are presented in Figs 10, 11, and 12.

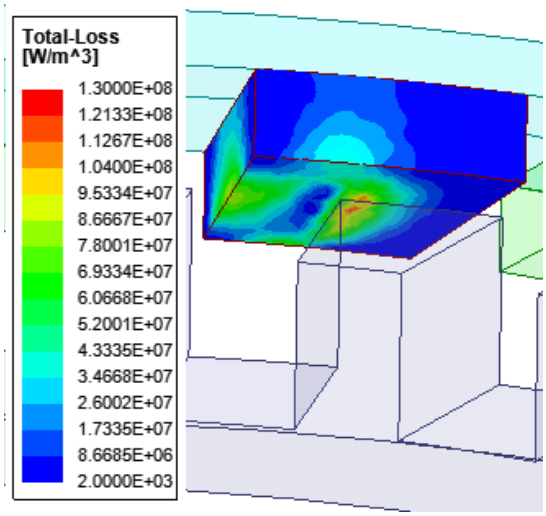

(a)

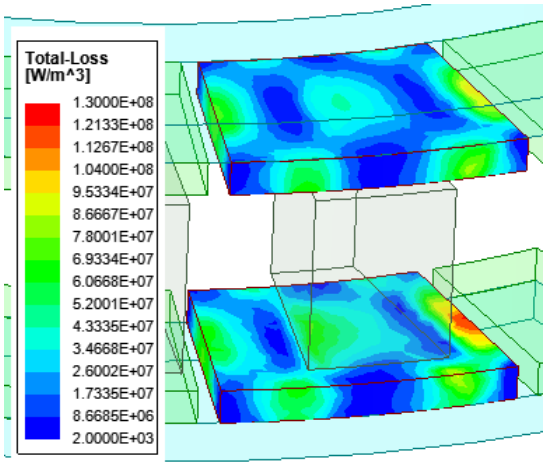

(b)

Fig. 9: The magnet eddy current losses for the selected optimal designs of the single sided AFPM and YASA topology.

TABLE II: Comparison of key parameters of optimised machines. Material costs taken from [25].

Parameter	Single-Sided	YASA
Power factor at full load	0.81	0.97
Average air gap flux density [T]	0.72	0.69
Current Density at full load [A/mm2]	14.6	15.1
DC Copper loss at peak torque [W]	439	536
No load core loss at 4000 rpm [W]	176	77
Bearing loss at 4000 rpm [W]	70	13
No load torque ripple (peak) [Nm]	0.2	0.44
Stator Core Mass [kg]	1.43	0.97
Rotor Core Mass [kg]	0.71	0.97
Copper Mass [kg]	1.30	1.51
Magnet Mass [kg]	0.77	0.74
Stator Core Cost [p.u.]	1.43	0.97
Rotor Core Cost [p.u.]	0.71	0.97
Copper Cost [p.u.]	3.90	4.54
Magnet Cost [p.u.]	18.54	17.87
Total Mass [kg]	4.22	4.20
Total Cost [p.u.]	24.6	24.3

Figure 10 presents both the additional losses due to the induced eddy currents at load and the DC copper loss. 3 turns are removed at each step, corresponding to a percentage reduction of the optimised copper content. Both topologies present similar results, with a 15% reduction in copper minimising the overall loss. The analysis was done on the initially selected winding. The large cross section of the wire demonstrates the importance of conductor proximity to the top of the slot. The YASA topology suffers more from this, as it features two air gaps. However, the increased magnet thickness in the single-sided design allows the magnet flux to penetrate deeper into the slot opening. As demonstrated in Figs. 11 and 12, whilst the YASA has higher overall loss, the loss in the single-sided is more concentrated, increasing hot spots in the top of the winding.

This paper focuses on the efficiency of electromagnetic power conversion for the two compared form factors, AC losses in windings and magnets weren't included in the original optimisation. AC Losses have been included for the two optimum designs to demonstrate the relative susceptibility to AC losses and the trade-off with DC losses, rather than to provide an absolute value. In a practical design, a smaller wire gauge would be chosen to reduce the effects of these AC losses. The exact winding arrangement depends on many application dependent parameters such as parallel coil paths, fill factor, duty cycle and torque constant, which cannot be covered generally.

The efficiency maps for the selected optimum designs are calculated with 3D FEA and shown in Fig. 13. The efficiency maps do not include windage, bearing or eddy current losses, as these were not considered in the optimisation. Differences in magnet eddy current losses are relatively negligible, assuming sufficient magnet segmentation. The YASA machine will have higher windage loss due to the two air gaps, however this is offset by the higher bearing loss in the single sided machine, due to the unbalanced attraction force. These losses scale differently with speed, so their effect depends on the intended duty cycle of the machine.

The 2D FEA AC loss investigation conducted in ANSYS

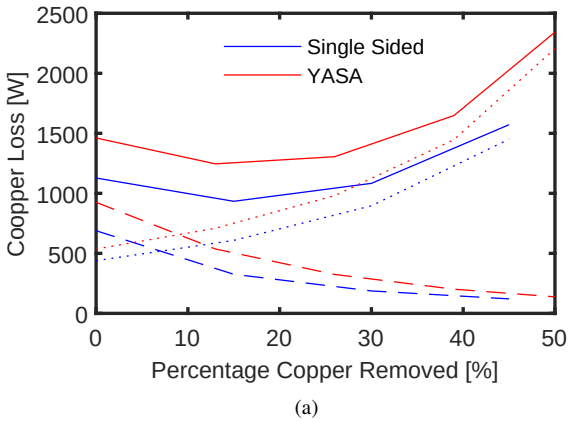

(a)

Fig. 10: The copper loss components and sum at 70Nm and 4000RPM for the chosen optimum YASA and Single-sided designs. The dotted lines are DC losses from excitation current, and the dashed lines are eddy current induced losses (from both excitation current and magnet passing). Removing turns decreases the latter, whilst increasing the DC losses due to the increased excitation current density.

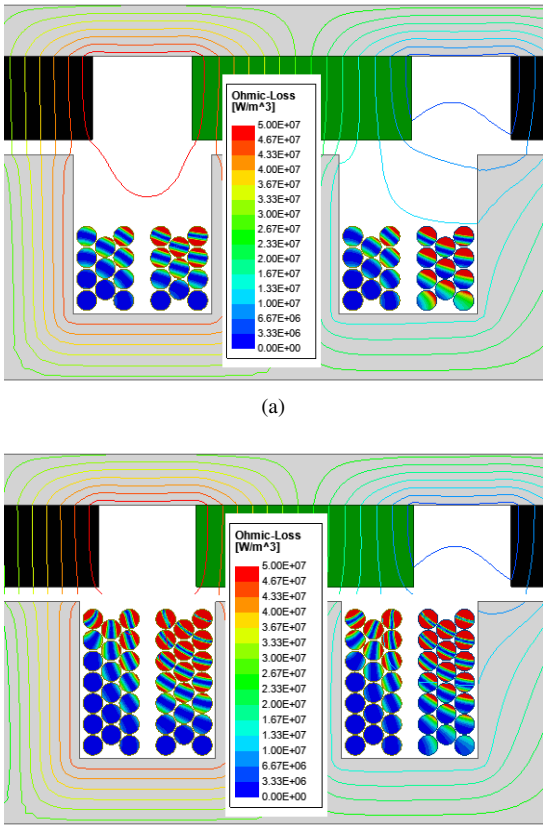

(a)

(b)

Fig. 11: The flux lines and total winding losses at the rated load of the selected single sided AFPM machine with (a) 11 and (b) 20 turns per coil. The current density is adjusted to generate the rated torque.

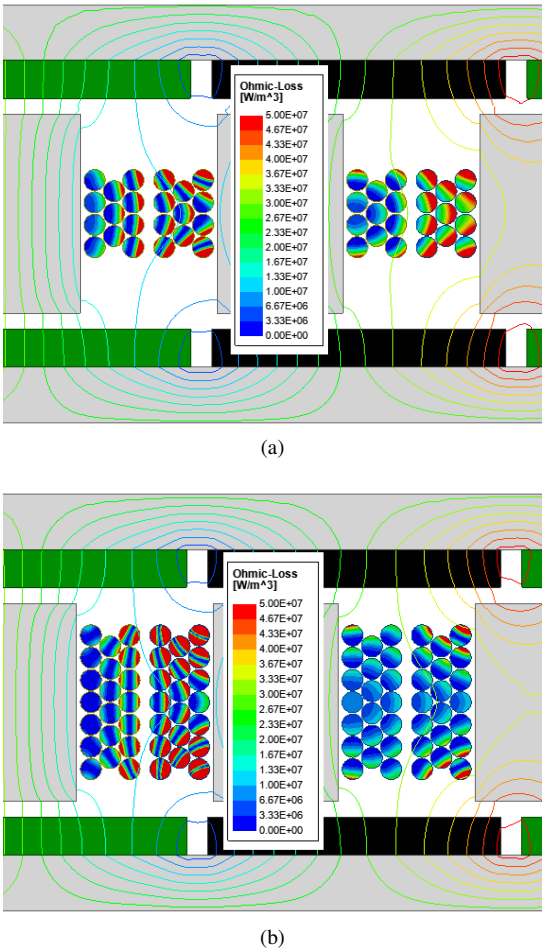

(a)

(b)

Fig. 12: The flux lines and total winding losses at the rated load of the selected YASA machine with (a) 11 and (b) 20 turns per coil. The current density is adjusted to generate the rated torque.

Maxwell highlights the importance of considering eddy currents in conductors, particularly for high frequency applications. Based on this analysis, the winding configuration for the prototype was modified to allow smaller diameter conductors. It indicates that a whilst the YASA machine is more susceptible to these losses, both topologies scale similarly.

In order to simplify the comparison of the two efficiency maps a third plot is obtained by subtracting them, presented in Fig. 13c. The positive values of this plot indicates higher efficiency of the single sided machine while the negative values show a higher efficiency for the YASA topology. It can be seen that for the two selected designs, assuming identical cooling methods, the single–stator single–rotor machine performs favorably at higher torque and lower speed operating points where the copper loss is more significant. Therefore, it may perform better for driving cycles with more torque requirement while the YASA machine is better for traction motors with higher speed and lower torque requirements. This picture is complicated somewhat by the AC winding losses, as the YASA machine AC losses tend to be higher. The degree to which this impacts the result of the optimisation depends on the ability of the machine designer to adequately design for these parasitic losses. A smaller cross sectional wire, litz wire, profile shaped windings or otherwise segmented windings will reduce the impact of these losses.

Another key difference between the two designs is the power factor under full load. The singled-sided machine has a much lower power factor (0.81) compared to the YASA machine (0.97). This is due to the large magnetising inductance of the single-sided machine, due to the inclusion of the stator yoke. Whilst this increases the inverter requirement, it is a necessary requirement for field weakening [26]. Therefore, the single-sided machine is attractive for applications requiring a high constant power speed range (CPSR) and fault tolerance, whereas the YASA machine is well suited to driving loads which don't require field weakening. In this case, as demonstrated in Fig. 14, the single-sided machine would be more suitable.

V. Experimental Validation

A single-sided prototype (Fig. 15) was constructed and tested under load. The application heavily prioritised mass over efficiency, so a design similar to those on the bottom right of (Fig. 4a) was selected. The design was also modified for practical vehicle packaging reasons.

The stator, depicted in Fig. 15c, is cooled through a water jacket that removes heat from the coil end turns and from the stator yoke into the aluminium housing. Using a lumped node thermal model, it was designed to have a continuous torque

capability of 45Nm, with a winding hot spot temperature of 155 C° and a coolant temperature of 75 C°. The motor can maintain peak torque of 70Nm for >60s depending on starting temperature. Similar concepts have been explored for YASA machines [16], [17] and would offer similar performance to the single-sided design. The stator core contact improves the cooling performance slightly when compared to a YASA style machine, however this is very dependent on geometry and slot insulation materials.

The N50H Magnets used in the rotor allow for rotor temperatures up to 120 C° in this design, but this is design specific, depending on the expected demagnetising fault currents and the magnetising inductance.

A sweep of efficiency points in steady state was completed from 500 to 3500 rpm, with the load varying from 2Nm to 20Nm due to inverter limitations. A Magtrol hysteresis brake was used for the load, with an N4L PPA3560 power analyser. Alongside dynamometer testing, back-EMF, spindown and DC resistance testing provide further validation of FEA simulation. This data was used to construct a loss separation model [27], and extrapolated to gain insight into the efficiency of the machine over its designed operating range (Fig. 17). Differences in efficiency can be noted between Figs 13a and 17. The motor in Fig. 13a balances efficiency and mass, whilst the motor in Fig. 17 prioritises low mass for a racing application. Additionally, the efficiency plots in Fig. 13 do not include bearing, windage and AC loss components, hence the notable efficiency discrepancy between the two figures. The testing shows close agreement for phase resistance and no-load spinning losses, with a slightly reduced back-EMF (Fig. 18). The simulation includes the effects of segmentation, which reduce active magnet material by about 5%. A summary comparing simulated and experimental results is presented in Table IV. Although the magnitude of the simulated and measured spinning losses are similar, the shape of the curves is different (Fig. 19). This could indicate either errors with hysteresis loss modelling in the core, or eddy current losses. An increase in hysteresis losses could possibly be caused by residual stresses in the steel from manufacturing, as the stators were not annealed after machining. This could also affect the permeability of the steel, further explaining the slightly reduced back-EMF. The majority of the simulated eddy current losses, including the AC resistance multiplier, are calculated from 2D analyses which have been extrapolated to account for eddy currents induced by rotor overhang. These analyses, whilst computationally efficient, have reduced accuracy when estimating complex 3D flux paths.

There is a slight discrepancy between the dynamometer no load losses and the losses extracted from the spindown testing. The origin of this is believed to be related to switching harmonics and inverter control, which are present throughout the dynamometer test data. This also explains the slight differences at the three listed efficiency points.

This design has a reasonable amount of spinning loss, prioritising a small air gap and reduced copper loss for a

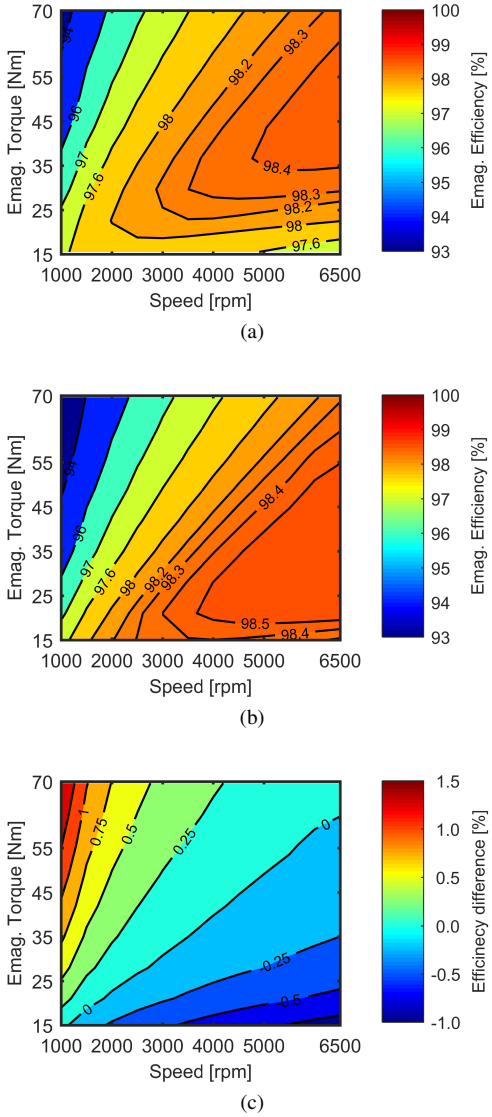

Fig. 13: The electromagnetic efficiency maps calculated by 3D FEA for the two representative designs with similar mass and loss: (a) single sided design, (b) the YASA design, and (c) the difference between efficiency maps of the two designs (the efficiency of the YASA machine subtracted from the single sided).

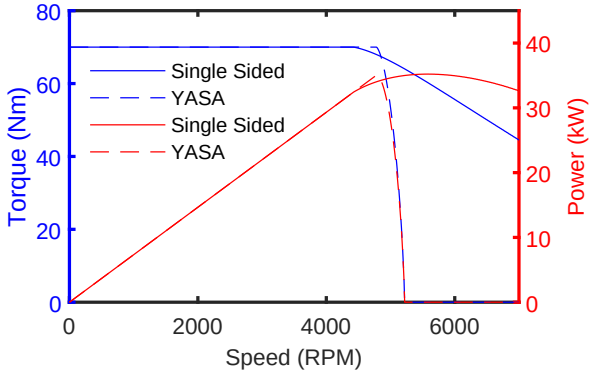

Fig. 14: The power and torque curves for the two optimised designs. The low power factor of the chosen YASA machine makes it a poor candidate for an application requiring a high CPSR.

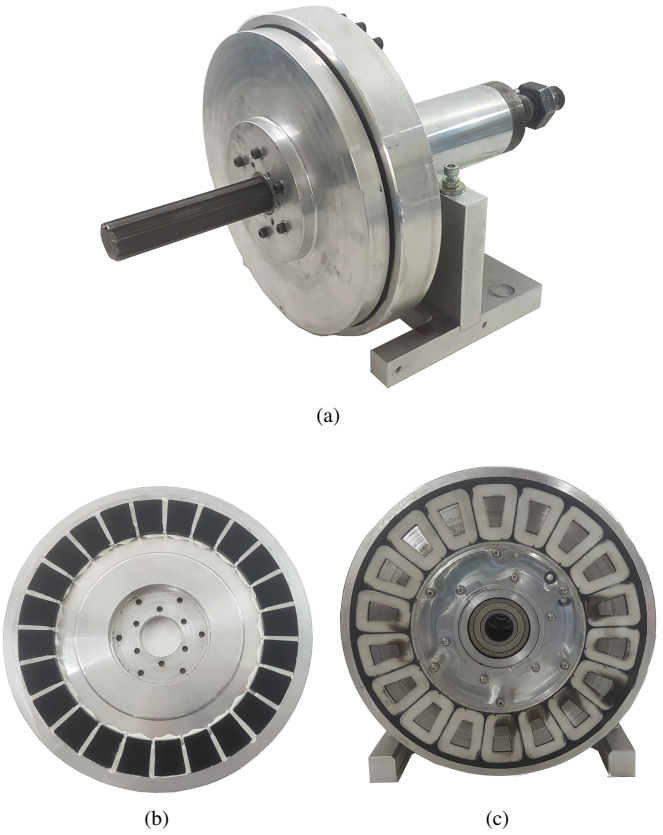

(a)

(b) (c)

Fig. 15: The motor designed for the vehicle application and experimental validation: (a) the assembled machine, (b) the rotor, (c) the stator.

(a) (b)

Fig. 16: A stator coil (a) and cross section (b) demonstrating the conductor location and a fill factor of 52% of the total slot area.

relatively high torque and low speed duty cycle. In addition to this, the manufactured coils (Fig. 16) have a high fill factor - ideal for low speed and high torque applications - but are placed reasonably high up in the slot, making them susceptible to magnet passing induced eddy currents. For an application requiring higher speeds, a design featuring a larger air gap or less conductors may be more suitable.

VI. Conclusion

This paper comparatively studies the performance of a YASA topology as opposed to a single–rotor single–stator AFPM machine for a formula student race car. Both machine types have been optimized to achieve minimum mass and electromagnetic loss within a given dimensional envelope.

TABLE III: Material specifications of prototype Motor.

Material	
Steel	Baosteel 250
Windings	0.95mm circular copper
Insulation	Polyester 200°C
Magnets	NdFeB N50H
Magnet segmentation	10 segments
Segment insulation thickness	0.1mm
Magnet content lost through segmentation	5.15%

TABLE IV: Comparison of Simulated and Experimental data.

Description	Simulated	Experimental
Torque Constant [Nm/A]	0.92	0.87
Phase Resistance at 60°C [mOhms]	56	59
AC Resistance Multiplier at 3500 RPM	1.12	-
Efficiency at 70Nm 2000 rpm	92%	90%
Efficiency at 40Nm 3500 rpm	94%	91%
Efficiency at 20Nm 4500 rpm	91%	89%
Spinning loss breakdown at 3500rpm		
Core [W]	196	-
Winding eddy current [W]	234	-
Magnet eddy current [W]	21	-
Cooling jacket eddy current [W]	14	-
Bearing [W]	44	-
Total no load loss [W]	508	560

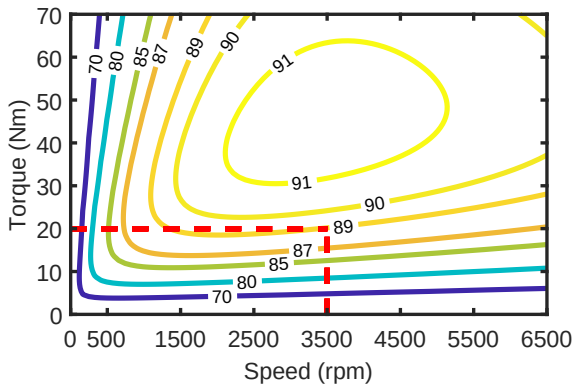

Fig. 17: Efficiency plot generated from experimental data. Dynamometer measurement within the red dashed lines.

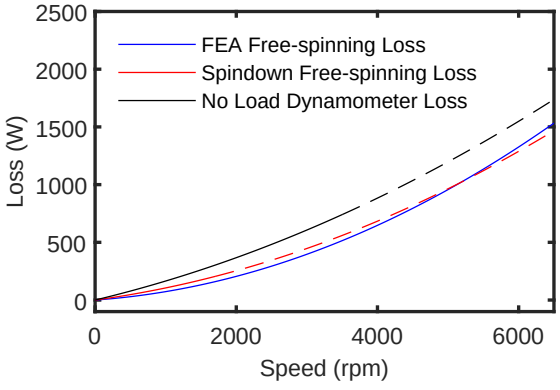

Fig. 18: Experimental and FEA back-EMF waveforms at 1700 rpm.

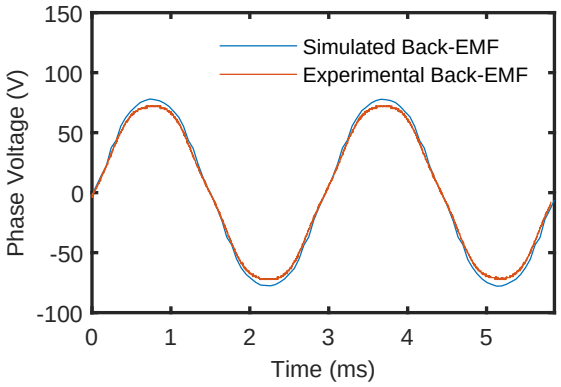

Fig. 19: Spinning loss from FEA, dynamometer and spindown testing - extrapolation shown as dashed line.

The very high efficiency YASA designs are lighter than their single sided counterparts of comparable torque and loss performance. On the other hand, single sided machines may be preferable for applications in which lower mass is of the essence, as they can also deal with the inevitably increased electromagnetic losses more effectively.

Within the entire design space considered, the optimally designed YASA machines require heavier copper windings and rotor cores, and lower stator core mass, as compared with the single–stator single–rotor machines. The YASA machines also require increasingly more magnet mass within the design space region with higher loss and lower mass. Lower core loss and higher copper loss are noted for the YASA optimal designs over the entire design space. The winding eddy current losses are comparable for the two machine configurations, while the YASA machines have higher magnet eddy current losses.

The studies conducted in this paper indicate that the preferred axial flux PM motor topology may depend on the torque and speed driving cycle requirements. The efficiency maps of two representative designs with comparable loss and mass show that, at the operating points with higher torque and lower speed, the single sided machine exhibits a higher efficiency, while for higher speed and lower torque, the YASA design is more efficient. A machine based on one of the generated optimum designs was built and tested, to demonstrate the validity of the analysis.

Acknowledgment

The support of Regal Beloit Corporation, ANSYS Inc., University of Kentucky, the L. Stanley Pigman endowment and the SPARK program is gratefully acknowledged.

Thanks to Max Schneider and Tim Pattinson for their work in constructing the prototype.

References

[1] F. Giulii Capponi, G. De Donato, and F. Caricchi, "Recent advances in axial-flux permanent-magnet machine technology," *IEEE Transactions on Industry Applications*, vol. 48, no. 6, pp. 2190–2205, 2012.

[2] P. D. Evans and J. F. Eastham, "Disc geometry homopolar synchronous machine," *IEE Proceedings*, vol. 127, no. 5, Sept 1980.

[3] E. Spooner and B. J. Chalmers, "Torus: A slotless, toroidal-stator, permanent-magnet generator," *IEE Proceedings*, vol. 139, no. 6, Nov 1992.

[4] T. J. Woolmer and M. D. McCulloch, "Analysis of the yokeless and segmented armature machine," in *2007 IEEE International Electric Machines Drives Conference*, vol. 1, May 2007, pp. 704–708.

[5] B. Zhang, T. Epskamp, M. Doppelbauer, and M. Gregor, "A comparison of the transverse, axial and radial flux pm synchronous motors for electric vehicle," in *2014 IEEE International Electric Vehicle Conference (IEVC)*, Dec 2014, pp. 1–6.

[6] N. J. Stannard, J. G. Washington, and G. J. Atkinson, "A comparison of axial field topologies employing smc for traction applications," in *2016 19th International Conference on Electrical Machines and Systems (ICEMS)*, Nov 2016, pp. 1–6.

[7] N. Taran, G. Heins, V. Rallabandi, D. Patterson, and D. M. Ionel, "Evaluating the effects of electric and magnetic loading on the performance of single- and double-rotor axial-flux pm machines," *IEEE Transactions on Industry Applications*, vol. 56, no. 4, pp. 3488–3497, 2020.

[8] N. J. Stannard, J. G. Washington, and G. J. Atkinson, "A comparison of axial field topologies employing smc for traction applications," in *2016 19th International Conference on Electrical Machines and Systems (ICEMS)*, 2016, pp. 1–6.

[9] B. Cheng, G. Pan, and Z. Mao, "Analytical calculation and optimization of the segmented-stator dual-rotor axial flux permanent magnet motors," *IEEE Transactions on Magnetics*, vol. 56, no. 11, pp. 1–9, 2020.

[10] T. Li, Y. Zhang, Y. Liang, Q. Ai, and H. Dou, "Multiphysics analysis of an axial-flux in-wheel motor with an amorphous alloy stator," *IEEE Access*, vol. 8, pp. 27 414–27 425, 2020.

[11] W. Geng, Z. Zhang, and Q. Li, "High torque density fractional-slot concentrated-winding axial-flux permanent-magnet machine with modular smc stator," *IEEE Transactions on Industry Applications*, vol. 56, no. 4, pp. 3691–3699, 2020.

[12] B. Zhang, T. Seidler, R. Dierken, and M. Doppelbauer, "Development of a yokeless and segmented armature axial flux machine," *IEEE Transactions on Industrial Electronics*, vol. 63, no. 4, pp. 2062–2071, April 2016.

[13] W. Fei, P. C. K. Luk, and K. Jinupun, "A new axial flux permanent magnet segmented-armature-torus machine for in-wheel direct drive applications," in *2008 IEEE Power Electronics Specialists Conference*, June 2008, pp. 2197–2202.

[14] W. Li, P. Song, S. Mukundan, B. De Silva Guruwatta Vidanalage, G. Spehar, V. Russalian, S. Reaburn, and N. C. Kar, "Structural analysis of single-sided axial-flux permanent magnet machines with different magnetic materials," *IEEE Transactions on Magnetics*, vol. 57, no. 2, pp. 1–5, 2021.

[15] H. Vansompel, P. Leijnen, and P. Sergeant, "Multiphysics analysis of a stator construction method in yokeless and segmented armature axial flux pm machines," *IEEE Transactions on Energy Conversion*, vol. 34, no. 1, pp. 139–146, 2019.

[16] R. Camilleri, D. A. Howey, and M. D. McCulloch, "Predicting the temperature and flow distribution in a direct oil-cooled electrical machine with segmented stator," *IEEE Transactions on Industrial Electronics*, vol. 63, no. 1, pp. 82–91, 2016.

[17] F. Marcolini, G. Dedonato, F. Giulii Capponi, and F. Caricchi, "Direct oil cooling of end-windings in torus-type axial-flux permanent-magnet machines," *IEEE Transactions on Industry Applications*, pp. 1–1, 2021.

[18] J. Chang, Y. Fan, J. Wu, and B. Zhu, "A yokeless and segmented armature axial flux machine with novel cooling system for in-wheel traction applications," *IEEE Transactions on Industrial Electronics*, vol. 68, no. 5, pp. 4131–4140, 2021.

[19] D. Winterborne, N. Stannard, L. Sjöberg, and G. Atkinson, "An air-cooled yasa motor for in-wheel electric vehicle applications," *IEEE Transactions on Industry Applications*, vol. 56, no. 6, pp. 6448–6455, 2020.

[20] M. Thiele and G. Heins, "Computationally efficient method for identifying manufacturing induced rotor and stator misalignment in permanent magnet brushless machines," *IEEE Transactions on Industry Applications*, vol. 52, no. 4, pp. 3033–3040, 2016.

[21] R. Z. Haddad, "Detection and identification of rotor faults in axial flux permanent magnet synchronous motors due to manufacturing and assembly imperfections," *IEEE Transactions on Energy Conversion*, vol. 35, no. 1, pp. 174–183, 2020.

[22] N. Taran, G. Heins, V. Rallabandi, D. Patterson, and D. M. Ionel, "Systematic comparison of two axial flux pm machine topologies: Yokeless and segmented armature versus single sided," in *2019 IEEE Energy Conversion Congress and Exposition (ECCE)*, 2019, pp. 4477–4482.

[23] N. Taran, D. M. Ionel, and D. G. Dorrell, "Two-level surrogate-assisted differential evolution multi-objective optimization of electric machines using 3-d fea," *IEEE Transactions on Magnetics*, vol. 54, no. 11, pp. 1–5, Nov 2018.
[24] C. E. Rasmussen and C. K. I. Williams, *Gaussian Processes for Machine Learning*. MIT Press, 2006.
[25] N. Taran, V. Rallabandi, G. Heins, and D. M. Ionel, "Systematically exploring the effects of pole count on the performance and cost limits of ultrahigh efficiency fractional hp axial flux pm machines," *IEEE Transactions on Industry Applications*, vol. 56, no. 1, pp. 117–127, 2020.
[26] W. Soong and T. Miller, "Theoretical limitations to the field-weakening performance of the five classes of brushless synchronous ac motor drive," in *1993 Sixth International Conference on Electrical Machines and Drives (Conf. Publ. No. 376)*, 1993, pp. 127–132.
[27] G. Heins, D. Ionel, D. Patterson, S. Stretz, and M. Thiele, "Combined experimental and numerical method for loss separation in permanent magnet brushless machines," *IEEE Transactions on Industry Applications*, vol. 52, pp. 1–1, 01 2015.